Journal of Innovations in Engineering Education
JIEE 2026, Vol. 9, Issue 1.

https://doi.org/10.3126/jiee.v9i1.90147

THAPATHALI CAMPUS
Institute of Engineering
Tribhuvan University

Development of transcendental mode shape functions of a pinned–pinned overhung beam with a lumped mass at the free overhung and an intermediate lumped mass

Bishal Kumar[a,b,*], Mahesh Chandra Luintel [a] and Surya Prasad Adhikari[a]

[a]*Department of Mechanical and Aerospace Engineering, Pulchowk Campus, Institute of Engineering, Tribhuvan University, Pulchowk, Lalitpur, Nepal*

[b]*Department of Automobile and Mechanical Engineering, Thapathali Campus, Institute of Engineering, Tribhuvan University, Thapathali, Kathmandu, Nepal*

ARTICLE INFO

Article history:

Received 28 January 2026
Revised in 12 February 2026
Accepted 5 April 2026

Keywords:

Pinned-pinned overhung
Transverse vibration
Euler-Bernoulli beam
Lumped mass
Transcendental

Abstract

This study presents the development of transcendental mode shape functions for a pinned–pinned overhung beam carrying a lumped mass at the free overhung end and an additional lumped mass located between the pinned supports. The beam is modeled as a slender Euler–Bernoulli beam, neglecting the effects of shear deformation and rotary inertia. The governing differential equation for free transverse vibration is solved analytically by imposing boundary conditions at the pinned supports and continuity and equilibrium conditions at the locations of the lumped masses, leading to the formulation of transcendental frequency equations and corresponding mode shapes. The first three bending vibration natural frequencies obtained from the analytical solution are 3.253 Hz, 13.769 Hz, and 103.329 Hz, respectively. To validate the analytical formulation, numerical simulations are performed using a finite element–based model. The corresponding simulated natural frequencies are found to be 4.167 Hz, 16.941 Hz, and 103.250 Hz.

1. Introduction

From truck axles and sandwich beam constructions to machine-tool assemblies, especially machine-tool spindle systems, beams in a variety of forms are essential for modelling a broad range of engineering systems. Optimizing structural weight, dynamic performance, and total cost requires precise assessment of the inherent frequencies of beam systems. Because double-span beam designs are frequently seen in real-world engineering applications beyond traditional single-span beams, they have garnered a lot of study interest. Because of its ease of use, Euler-Bernoulli beam theory is one of the most often used analytical techniques for the vibration analysis of beam-like structures.

Due to its importance in real-world engineering applications, such as machine-tool spindles, overhung shafts, bridges, and aerospace structures, the free vibration analysis of beam structures containing discrete attachments, such as lumped masses, has been extensively researched. Compared to uniform beams, lumped masses alter natural frequencies and mode shapes by introducing discontinuities in inertia. For design optimization, weight reduction, and dynamic performance increase, accurate prediction of these characteristics is crucial [1].

By splitting the slender beam into spans at mass locations and expressing the transverse displacement as a combination of Euler–Bernoulli solutions with hyperbolic and trigonometric functions, the natural frequencies and mode shapes of a uniform multi-span beam carrying multiple point masses have been examined. In order to accurately describe the effect of discrete masses on modal curvature, global mode shapes are assembled using continuity and equilibrium conditions at the mass sites [2].

In Euler-Bernoulli beams with numerous particles, piecewise mode shape functions have also been used.

*Corresponding author:
jhabishal12@gmail.com (B. Kumar)

In these beams, each beam segment is represented by base functions that satisfy the beam equation, and the coefficients are found using continuity and jump conditions at the particle locations. This method highlights the necessity for accurate segment-wise mode shape construction by showing that discrete masses have a considerable impact on local curvature and overall vibration characteristics [3].

By using frequency-dependent stiffness matrices, the dynamic stiffness method (DSM) offers a precise way to create mode forms that naturally satisfy boundary constraints and take mass or stiffness discontinuities into consideration. DSM is very useful for analyzing beams with many mass points or structural imperfections and does not require assumed basis functions [4].

Piecewise transcendental mode functions have been derived for each segment of beams carrying two point masses. According to the study, the mode shapes exhibit obvious distortions close to mass spots, and the second and third natural frequencies shift when compared to a bare beam, demonstrating the necessity of analytical functions for an accurate modelling of discrete mass effects [5].

An analytical investigation of a simply supported beam with an overhang holding a point mass at the free end was presented. This configuration was pertinent to boring bars and machine tool spindles. By applying boundary and continuity criteria at the overhang, they used Euler-Bernoulli beam theory to develop closed-form formulas for natural frequencies and mode shapes. Finite element analysis was used to evaluate the results, and the results indicated good agreement. A useful tool for vibration analysis and the design of overhung beam-mass systems, the study showed that the analytical solution could effectively forecast dynamic behavior and optimize mass and support placement without the need for lengthy numerical simulations [1].

The practical significance of modal modelling was demonstrated by parameter identification for complex mechanical systems, such as fire truck suspensions, which showed that precise estimation of system parameters allows predicted vibration amplitudes and mode shapes to match measurements within 5% error [6].

Polynomial mode shape functions have been proposed for continuous shafts to simplify classical transcendental solutions. These polynomial functions are constructed to satisfy boundary conditions and approximate physical mode shapes for low-order modes, providing an alternative for systems where exact solutions are difficult to handle analytically [7].

Using Lagrange's equation and the assumed mode approach, the application of polynomial mode shape functions to the free vibration analysis of a cantilever Pelton turbine has been studied. Conventional transcendental mode forms were compared with the polynomial functions. According to the data, the first crucial frequency deviated by 2.23%, rising to 14.58% in the second mode and 20.53% in the third. Although polynomial mode shapes provide computational simplicity and an accurate approximation of the basic mode, their accuracy sharply declines for higher modes in intricate rotor-dynamic systems [8].

The free vibration of Euler-Bernoulli beams on elastic foundations has been approximated using He's variational iteration approach. Semi-analytical iterative approaches have been shown to reliably yield accurate mode shapes, as evidenced by the first natural frequencies obtained agreeing with FEM solutions within 3–4% [9].

The first three natural frequencies of adaptive polynomial mode functions for L-type beams with free ends have been verified to match FEM results within 2–3%, demonstrating better accuracy for difficult geometries than standard polynomials [10].

Functionally graded beams have also been subjected to the dynamic stiffness approach, which yields closed-form, precise mode shapes and natural frequencies. This spectral approach provides a template for precisely determining transcendental mode functions in non-homogeneous beams while rigorously satisfying boundary requirements and taking material quality fluctuations into consideration [11].

Lastly, mode forms have been approximated using trigonometric and Fourier-based basis functions, particularly for oscillatory or higher-order structures. Compared to basic polynomial bases, sine/cosine expansions and enriched trigonometric interpolations offer good solutions to complicated geometries [12].

The explicit derivation of transcendental mode shape functions for pinned-pinned overhung beams carrying both an intermediate lumped mass and an overhung end mass has received little attention, despite the substantial study on beams with single or intermediate lumped masses. The current study uses Euler-Bernoulli beam theory to establish precise transcendental mode shape functions and natural frequency equations for such beam systems because the combined impacts of overhang geometry and multiple inertia discontinuities enhance analytical complexity.

2. Research methodology

Using Euler-Bernoulli beam theory, the analytical process is built under the presumptions of neglecting shear deformation and rotational inertia. The beam domain is divided at the concentrated mass points, and the governing fourth-order differential equation of free vibration is developed. Each segment has closed-form solutions, and the unknown constants are found by applying pinned support conditions, together with slope and displacement continuity, and dynamic equilibrium at the lumped mass sites. The natural frequencies are obtained from the roots of a transcendental characteristic equation that results from this method, and the associated mode shapes are obtained by substituting these values.

The beam and its discrete mass attachments were modelled using a finite element description of the structural configuration for numerical analysis. Concentrated masses were placed at the designated intermediate and overhung locations, and the supports were designed to replicate optimal pinning circumstances. To preserve consistency throughout the computational domain, a structured discretization approach was used.

The mesh quality examination revealed a skewness score of 1.328×10^{-10}, suggesting little element distortion. The model has 200,000 elements with a consistent element size. The first three bending natural frequencies and their associated mode shapes were then extracted using an eigenvalue-based modal analysis, and they were then utilised to compare with the analytical findings.

3. Free vibration analysis

Figure 1 illustrates a pinned–pinned overhung beam carrying a lumped mass at the free overhung end and another lumped mass located between the pinned supports. The beam is assumed to be uniform, slender, and subjected to transverse vibration.

Since the scope of the present study is limited to the free vibration analysis of a uniform beam, the governing differential equation is formulated based on the classical Euler–Bernoulli beam theory as shown in Equation 1 [13]. In this formulation, the effects of shear deformation and rotary inertia are neglected, which is a reasonable assumption for beams that are slender in nature [14].

$$EI\frac{\partial^4 w(x,t)}{\partial x^4} + \rho A\frac{\partial^2 w(x,t)}{\partial t^2} = 0 \tag{1}$$

Where E is the Young's Modulus, I is the moment of inertia of the beam cross-section, $w(x,t)$ is the vertical deflection, t is time, ρ is the density of the beam material, and A is the cross-sectional area of the beam.

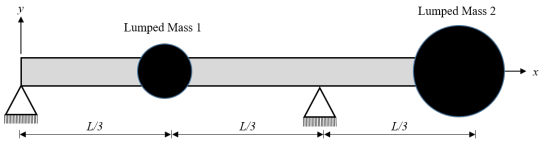

Figure 1: Pinned-pinned overhung beam

The solution of Equation 1 is obtained using the method of separation of variables. Under the deployment of the method of separation of variables [15], the solution of Equation 1 takes the form,

$$w(x,t) = X(x)\,T(t) \tag{2}$$

The solution of the spatial term of Equation 2 can be written in piecewise form for the problem geometry shown in Figure 1 as,

$$X(x) = \begin{cases} X_1(x), & 0 \le x \le \frac{L}{3} \\ X_2(x), & \frac{L}{3} \le x \le \frac{2L}{3} \\ X_3(x), & \frac{2L}{3} \le x \le L \end{cases} \tag{3}$$

$X_1(x)$, $X_2(x)$, and $X_3(x)$ can be expressed in terms of a transcendental equation as,

$$X_1(x) = a\sin(\beta x)+b\cos(\beta x)+c\sinh(\beta x)+d\cosh(\beta x) \tag{4}$$

$$X_2(x) = e\sin(\beta x)+f\cos(\beta x)+g\sinh(\beta x)+h\cosh(\beta x) \tag{5}$$

$$X_3(x) = i\sin(\beta x)+j\cos(\beta x)+k\sinh(\beta x)+l\cosh(\beta x) \tag{6}$$

In Equation 4, Equation 5, and Equation 6, β represents the eigenvalue in the beam's bending vibration.

3.1. Boundary conditions and development of non-trivial equations

For the problem presented in Figure 1, the boundary conditions moving from left to right are determined at the first pin, the second pin, the point of application of lumped mass 1, and the free end (point of application of lumped mass 2).

At the left pin, deflection and moment are equal to zero.

$$X_1(0) = 0 \tag{7}$$

$$\frac{d^2X_1(0)}{dx^2} = 0 \tag{8}$$

At the point of application of lumped mass 1 in between the pins, there exists continuity in deflection, slope, and moment values, followed by a jump in shear force.

$$X_1\left(\frac{L}{3}\right) - X_2\left(\frac{L}{3}\right) = 0 \tag{9}$$

$$\frac{dX_1\left(\frac{L}{3}\right)}{dx} - \frac{dX_2\left(\frac{L}{3}\right)}{dx} = 0 \tag{10}$$

$$\frac{d^2X_1\left(\frac{L}{3}\right)}{dx^2} - \frac{d^2X_2\left(\frac{L}{3}\right)}{dx^2} = 0 \tag{11}$$

$$\frac{d^3X_2\left(\frac{L}{3}\right)}{dx^3} - \frac{d^3X_1\left(\frac{L}{3}\right)}{dx^3} - \frac{m_1\beta^4}{\rho A}X_1\left(\frac{L}{3}\right) = 0 \tag{12}$$

At the right pin, deflection is zero, followed by continuity in values of slope and moment.

$$X_2\left(\frac{2L}{3}\right) = 0 \tag{13}$$

$$X_3\left(\frac{2L}{3}\right) = 0 \tag{14}$$

$$\frac{dX_2\left(\frac{2L}{3}\right)}{dx} - \frac{dX_3\left(\frac{2L}{3}\right)}{dx} = 0 \tag{15}$$

$$\frac{d^2X_2\left(\frac{2L}{3}\right)}{dx^2} - \frac{d^2X_3\left(\frac{2L}{3}\right)}{dx^2} = 0 \tag{16}$$

Similarly, at the free end moment value is zero, followed by a jump in shear force values.

$$\frac{d^2X_3(L)}{dx^2} = 0 \tag{17}$$

$$\frac{d^3X_3(L)}{dx^3} - \frac{m_2\beta^4}{\rho A}X_3(L) = 0 \tag{18}$$

The boundary conditions, when substituted in Equation 4, Equation 5, and Equation 6, lead to the development of new sets of equations as shown below.

$$b + d = 0 \tag{19}$$

$$b - d = 0 \tag{20}$$

$$\begin{aligned} &a\sin\left(\frac{\beta L}{3}\right) + b\cos\left(\frac{\beta L}{3}\right) + c\sinh\left(\frac{\beta L}{3}\right) \\ &+ d\cosh\left(\frac{\beta L}{3}\right) - e\sin\left(\frac{\beta L}{3}\right) - f\cos\left(\frac{\beta L}{3}\right) \\ &- g\sinh\left(\frac{\beta L}{3}\right) - h\cosh\left(\frac{\beta L}{3}\right) = 0 \end{aligned} \tag{21}$$

$$\begin{aligned} &a\cos\left(\frac{\beta L}{3}\right) - b\sin\left(\frac{\beta L}{3}\right) + c\cosh\left(\frac{\beta L}{3}\right) \\ &+ d\sinh\left(\frac{\beta L}{3}\right) - e\cos\left(\frac{\beta L}{3}\right) + f\sin\left(\frac{\beta L}{3}\right) \\ &- g\cosh\left(\frac{\beta L}{3}\right) - h\sinh\left(\frac{\beta L}{3}\right) = 0 \end{aligned} \tag{22}$$

$$\begin{aligned} &-a\sin\left(\frac{\beta L}{3}\right) - b\cos\left(\frac{\beta L}{3}\right) + c\sinh\left(\frac{\beta L}{3}\right) \\ &+ d\cosh\left(\frac{\beta L}{3}\right) + e\sin\left(\frac{\beta L}{3}\right) + f\cos\left(\frac{\beta L}{3}\right) \\ &- g\sinh\left(\frac{\beta L}{3}\right) - h\cosh\left(\frac{\beta L}{3}\right) = 0 \end{aligned} \tag{23}$$

$$\begin{aligned} &a\left[\cos\left(\frac{\beta L}{3}\right) - \frac{m_1\beta}{\rho A}\sin\left(\frac{\beta L}{3}\right)\right] \\ &+ b\left[-\sin\left(\frac{\beta L}{3}\right) - \frac{m_1\beta}{\rho A}\cos\left(\frac{\beta L}{3}\right)\right] \\ &+ c\left[-\cosh\left(\frac{\beta L}{3}\right) - \frac{m_1\beta}{\rho A}\sinh\left(\frac{\beta L}{3}\right)\right] \\ &+ d\left[-\sinh\left(\frac{\beta L}{3}\right) - \frac{m_1\beta}{\rho A}\cosh\left(\frac{\beta L}{3}\right)\right] \\ &- e\cos\left(\frac{\beta L}{3}\right) - f\sin\left(\frac{\beta L}{3}\right) + g\cosh\left(\frac{\beta L}{3}\right) \\ &+ h\sinh\left(\frac{\beta L}{3}\right) = 0 \end{aligned} \tag{24}$$

$$\begin{aligned} &e\sin\left(\frac{2\beta L}{3}\right) + f\cos\left(\frac{2\beta L}{3}\right) + g\sinh\left(\frac{2\beta L}{3}\right) \\ &+ h\cosh\left(\frac{2\beta L}{3}\right) = 0 \end{aligned} \tag{25}$$

$$i\sin\left(\frac{2\beta L}{3}\right)+j\cos\left(\frac{2\beta L}{3}\right)+k\sinh\left(\frac{2\beta L}{3}\right)+l\cosh\left(\frac{2\beta L}{3}\right)=0 \tag{26}$$

$$e\cos\left(\frac{2\beta L}{3}\right)-f\sin\left(\frac{2\beta L}{3}\right)+g\cosh\left(\frac{2\beta L}{3}\right)+h\sinh\left(\frac{2\beta L}{3}\right)-i\cos\left(\frac{2\beta L}{3}\right)+j\sin\left(\frac{2\beta L}{3}\right)-k\cosh\left(\frac{2\beta L}{3}\right)-l\sinh\left(\frac{2\beta L}{3}\right)=0 \tag{27}$$

$$-e\sin\left(\frac{2\beta L}{3}\right)-f\cos\left(\frac{2\beta L}{3}\right)+g\sinh\left(\frac{2\beta L}{3}\right)+h\cosh\left(\frac{2\beta L}{3}\right)+i\sin\left(\frac{2\beta L}{3}\right)+j\cos\left(\frac{2\beta L}{3}\right)-k\sinh\left(\frac{2\beta L}{3}\right)-l\cosh\left(\frac{2\beta L}{3}\right)=0 \tag{28}$$

$$-i\sin(\beta L)-j\cos(\beta L)+k\sinh(\beta L)+l\cosh(\beta L)=0 \tag{29}$$

$$\begin{aligned} &i\left[-\cos(\beta L)+\frac{m_2\beta}{\rho A}\sin(\beta L)\right]\\ &+j\left[\sin(\beta L)+\frac{m_2\beta}{\rho A}\cos(\beta L)\right]\\ &+k\left[\cosh(\beta L)+\frac{m_2\beta}{\rho A}\sinh(\beta L)\right]\\ &+l\left[\sinh(\beta L)+\frac{m_2\beta}{\rho A}\cosh(\beta L)\right]=0 \end{aligned} \tag{30}$$

The above sets of equations from Equation 19 to Equation 30 lead to the development of equations that have non trivial solution.

Accommodating all coefficients at a time in a 12 by 12 matrix is somehow complicated; this issue can be addressed greatly using the concept of matrix partitioning.

$$\text{Coefficient matrix}=\begin{bmatrix}A & B\\ C & D\end{bmatrix} \tag{31}$$

Solving the coefficient matrix using Maple, the value of βL can be obtained for the parameter values as shown in Table 1.

Table 1: Value of beam parameters

Parameters	Values
Length of beam (L)	1 m
Density of beam material (ρ)	7850 kg/m^3
Young's Modulus (E)	200 GPa
Lumped Mass 1	0.314 kg
Lumped Mass 2	0.628 kg
Area of beam cross-section (A)	25 mm^2
Moment of Inertia (I)	52.083 mm^4

The obtained value of βL for the first three modes is found to be 1.675, 3.446, and 9.440, respectively, and the corresponding natural frequency can be obtained from the relation,

$$f_n=\frac{\beta_n^2}{2\pi}\sqrt{\frac{EI}{\rho A}} \tag{32}$$

The natural frequencies corresponding to the first three modes are found to be 3.253 Hz, 13.769 Hz, and 103.329 Hz, respectively.

3.2. Mode shapes

The coefficients a, b, c, d, e, f, g, h, i, j, k, and l must be found in order to derive the mode forms. Nevertheless, the equations are insufficient to calculate the value of the coefficients. Therefore, all of the coefficients are normalized by dividing by a coefficient in order to determine the value of each coefficient.

When the value of βL is substituted in the above sets of equations from Equation 19 to Equation 30, the value of normalized coefficients is obtained, which leads to the development of the piecewise transcendental mode shapes equation as shown below. The mode shapes are denoted as $X(x)_{\text{First mode}}$, $X(x)_{\text{Second mode}}$, and $X(x)_{\text{Third mode}}$, respectively.

The first three mode shapes obtained are shown in Figure 2.

4. Model validation using FEA

The same problem was solved using ANSYS to find the first three mode shapes, which are obtained as shown in Figure 3, Figure 4, and Figure 5, which correspond to the natural frequencies of 4.167 Hz, 16.941 Hz, and 103.250 Hz, respectively. One node is visible in the first mode, two in the second, and three in the third. In the first mode, the overhung section of the beam exhibits a noticeable elastic curve, but in higher modes, its impact lessens. Higher modes are characterized by homogeneous bending patterns rather than overhung

$$A=\begin{bmatrix} 0 & 1 & 0 & 1 & 0 & 0 \\ 0 & 1 & 0 & -1 & 0 & 0 \\ \sin(\beta L/3) & \cos(\beta L/3) & \sinh(\beta L/3) & \cosh(\beta L/3) & -\sin(\beta L/3) & -\cos(\beta L/3) \\ \cos(\beta L/3) & -\sin(\beta L/3) & \cosh(\beta L/3) & \sinh(\beta L/3) & -\cos(\beta L/3) & \sin(\beta L/3) \\ -\sin(\beta L/3) & -\cos(\beta L/3) & \sinh(\beta L/3) & \cosh(\beta L/3) & \sin(\beta L/3) & \cos(\beta L/3) \\ \cos(\beta L/3)-\frac{m_1\beta}{\rho A}\sin(\beta L/3) & -\sin(\beta L/3)-\frac{m_1\beta}{\rho A}\cos(\beta L/3) & -\cosh(\beta L/3)-\frac{m_1\beta}{\rho A}\sinh(\beta L/3) & -\sinh(\beta L/3)-\frac{m_1\beta}{\rho A}\cosh(\beta L/3) & -\cos(\beta L/3) & -\sin(\beta L/3) \end{bmatrix}$$

$$B=\begin{bmatrix} 0 & 0 & 0 & 0 & 0 & 0 \\ 0 & 0 & 0 & 0 & 0 & 0 \\ -\sinh(\beta L/3) & -\cosh(\beta L/3) & 0 & 0 & 0 & 0 \\ -\cosh(\beta L/3) & -\sinh(\beta L/3) & 0 & 0 & 0 & 0 \\ -\sinh(\beta L/3) & -\cosh(\beta L/3) & 0 & 0 & 0 & 0 \\ \cosh(\beta L/3) & \sinh(\beta L/3) & 0 & 0 & 0 & 0 \end{bmatrix}$$

$$C=\begin{bmatrix} 0 & 0 & 0 & 0 & \sin(2\beta L/3) & \cos(2\beta L/3) \\ 0 & 0 & 0 & 0 & 0 & 0 \\ 0 & 0 & 0 & 0 & \cos(2\beta L/3) & -\sin(2\beta L/3) \\ 0 & 0 & 0 & 0 & -\sin(2\beta L/3) & -\cos(2\beta L/3) \\ 0 & 0 & 0 & 0 & 0 & 0 \\ 0 & 0 & 0 & 0 & 0 & 0 \end{bmatrix}$$

$$D=\begin{bmatrix} \sinh(2\beta L/3) & \cosh(2\beta L/3) & 0 & 0 & 0 & 0 \\ 0 & 0 & \sin(2\beta L/3) & \cos(2\beta L/3) & \sinh(2\beta L/3) & \cosh(2\beta L/3) \\ \cosh(2\beta L/3) & \sinh(2\beta L/3) & -\cos(2\beta L/3) & \sin(2\beta L/3) & -\cosh(2\beta L/3) & -\sinh(2\beta L/3) \\ \sinh(2\beta L/3) & \cosh(2\beta L/3) & \sin(2\beta L/3) & \cos(2\beta L/3) & -\sinh(2\beta L/3) & -\cosh(2\beta L/3) \\ 0 & 0 & -\sin(\beta L) & -\cos(\beta L) & \sinh(\beta L) & \cosh(\beta L) \\ 0 & 0 & -\cos(\beta L)+\frac{m_2\beta}{\rho A}\sin(\beta L) & \sin(\beta L)+\frac{m_2\beta}{\rho A}\cos(\beta L) & \cosh(\beta L)+\frac{m_2\beta}{\rho A}\sinh(\beta L) & \sinh(\beta L)+\frac{m_2\beta}{\rho A}\cosh(\beta L) \end{bmatrix}$$

$$X(x)_{\text{First mode}}=\begin{cases} \sin(1.675084339x)-0.6668328397\sinh(1.675084339x), & 0\le x\le \frac{L}{3} \\ 0.8433698218\sin(1.675084339x)+0.09784205788\cos(1.675084339x) & \\ \quad -0.4526104174\sinh(1.675084339x)-0.1085595008\cosh(1.675084339x), & \frac{L}{3}\le x\le \frac{2L}{3} \\ -0.05713964771\sin(1.675084339x)+1.942812108\cos(1.675084339x) & \\ \quad +3.019204271\sinh(1.675084339x)-2.908321175\cosh(1.675084339x), & \frac{2L}{3}\le x\le L \end{cases}$$

$$X(x)_{\text{Second mode}}=\begin{cases} \sin(3.446261836x)-0.2926785813\sinh(3.446261836x), & 0\le x\le \frac{L}{3} \\ 0.4386552372\sin(3.446261836x)+1.250142912\cos(3.446261836x) & \\ \quad +2.085830873\sinh(3.446261836x)-1.944052978\cosh(3.446261836x), & \frac{L}{3}\le x\le \frac{2L}{3} \\ -0.5546460784\sin(3.446261836x)+0.1328347022\cos(3.446261836x) & \\ \quad -5.426443908\sinh(3.446261836x)+5.417960826\cosh(3.446261836x), & \frac{2L}{3}\le x\le L \end{cases}$$

$$X(x)_{\text{Third mode}}=\begin{cases} \sin(9.440797619x)+0.0003548462916\sinh(9.440797619x), & 0\le x\le \frac{L}{3} \\ 0.9907873456\sin(9.440797619x)+0.00004919488039\cos(9.440797619x) & \\ \quad -0.1070090140\sinh(9.440797619x)+0.1069678599\cosh(9.440797619x), & \frac{L}{3}\le x\le \frac{2L}{3} \\ 0.9698352842\sin(9.440797619x)+0.0002727793044\cos(9.440797619x) & \\ \quad +5.563327905\sinh(9.440797619x)-5.563330346\cosh(9.440797619x), & \frac{2L}{3}\le x\le L \end{cases}$$

deflection, and the deformation over the main span becomes more sinusoidal as the mode number rises. This pattern demonstrates how, in higher vibration modes, overhung-dominated behavior gives way to classical bending characteristics.

5. Results and discussion

The finite element simulation predicts corresponding values of 4.167 Hz, 16.941 Hz, and 103.250 Hz, while the analytical solution returns the first three bending natural frequencies as 3.253 Hz, 13.769 Hz, and 103.329 Hz. While the third mode exhibits extremely tight agreement between the two methods, the discrepancy is found

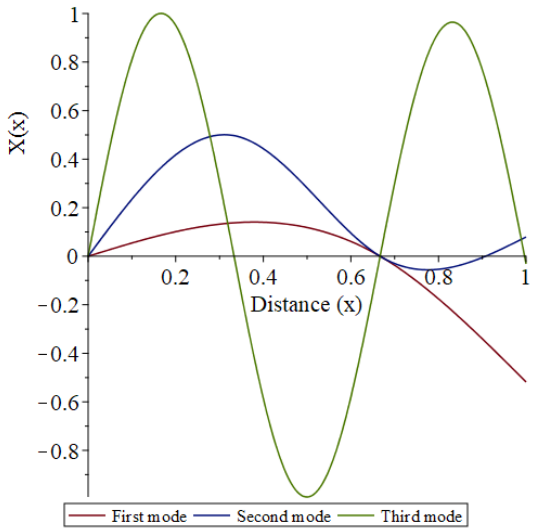

Figure 2: Mode shapes obtained through analytical solution

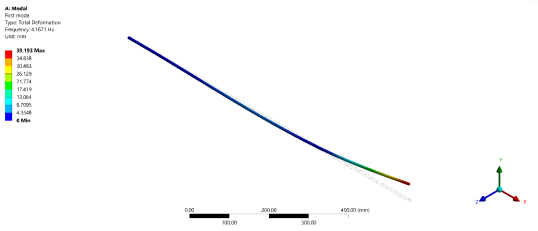

Figure 3: First mode obtained through simulation

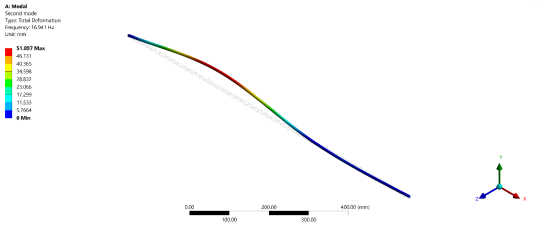

Figure 4: Second mode obtained through simulation

to be substantial for the lower modes.

These variations mostly result from the underlying presumptions and modelling techniques used in each approach. The idealized Euler-Bernoulli beam theory serves as the basis for the analytical formulation, which ignores shear deformation, rotating inertia, and localized stiffness or mass effects while assuming a continuous system with simplified boundary conditions. The structure is represented by discrete elements in the finite element model, which also includes a more thorough numerical depiction of the mass distribution and boundary conditions at nodal positions. These elements can

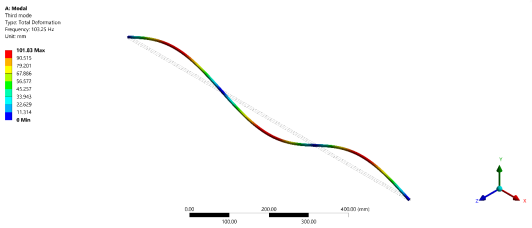

Figure 5: Third mode obtained through simulation

have a greater impact on the lower natural frequencies, as might be estimated from eigenvalue solvers.

The mode shapes derived from both methods show significant agreement despite the difference in frequency values. The bending modes' curvature distributions, nodal locations, and deformation patterns are all consistent between the numerical and analytical models. This consistency in mode shape features supports the validity of the numerical model for this inquiry by confirming that the simulation accurately depicts the beam's basic dynamic behavior.

In addition to this, a parametric study was also observed qualitatively by varying the magnitude of the lumped masses. The results indicate that increasing the lumped mass values leads to a reduction in the natural frequencies, while the mode shapes follow trends similar to the original case. Conversely, reducing the lumped masses results in higher natural frequencies, with greater distortion observed, particularly for the higher modes, compared to the original case.

6. Conclusion

The vibration of a pinned–pinned overhung beam with an intermediate and a free overhung lumped mass is analyzed in this work using a transcendental mode shape formulation. Higher-mode natural frequencies closely agree, according to analytical and numerical studies, while the first mode shows a greater disagreement because it is more sensitive to modelling assumptions. The first mode's percentage deviation from the simulation results is about 28.1%, the second mode's is about 23.0%, and the third mode's is about 0.08%. The mode forms from the two methods exhibit good agreement in curvature and nodal positions in spite of these differences. These findings complement upcoming computational and experimental beam dynamics research by validating the suggested framework and proving its effectiveness in forecasting bending frequencies and mode shapes.

Future studies could extend this work by incorporating shear deformation and rotary inertia effects to assess

their influence on lower-mode frequencies, particularly the first mode. The accuracy of the model might be further increased through experimental validation using physical prototypes, which could also reveal information on damping effects and actual boundary conditions. Furthermore, parametric research on different lumped mass locations, beam geometries, and material properties could improve our comprehension of the dynamics of overhung beams and direct the development of optimal designs for engineering applications.

Acknowledgements

The authors declare that no specific funding, grant, or financial support was received from any public, commercial, or not-for-profit funding agencies for the conduct of this research.

Conflict of interest

The authors state that there are no known competing financial interests or personal relationships that could have influenced the outcomes of this study.

References

[1] Alzghoul M, Cabezas S, Szilágyi A. Dynamic modeling of a simply supported beam with an overhang mass[J/OL]. Pollack Periodica, 2022, 17(2): 42-47. DOI: 10.1556/606.2022.00523.

[2] Lin H Y, Tsai Y C. On the natural frequencies and mode shapes of a uniform multi-span beam carrying multiple point masses[J/OL]. Structural Engineering and Mechanics, 2005, 21 (3): 351-367. DOI: 10.12989/sem.2005.21.3.351.

[3] Naguleswaran S. Transverse vibrations of an Euler–Bernoulli uniform beam carrying several particles[J/OL]. International Journal of Mechanical Sciences, 2002, 44(12): 2463-2478. DOI: 10.1016/S0020-7403(02/00182-0.

[4] Banerjee J R. Dynamic stiffness formulation for structural elements: A general approach[J/OL]. Computers & Structures, 1997, 63(1): 101-103. DOI: 10.1016/S0045-7949(96/00326-4.

[5] Naguleswaran S. Transverse vibrations of an Euler–Bernoulli uniform beam carrying two particles in-span[J/OL]. International Journal of Mechanical Sciences, 2001, 43(12): 2737-2752. DOI: 10.1016/S0020-7403(01/00072-8.

[6] Hajdu F, Szalai P, Mika P, et al. Parameter identification of a fire truck suspension for vibration analysis[J/OL]. Pollack Periodica, 2019, 14(3): 51-62. DOI: 10.1556/606.2019.14.3.6.

[7] Luintel M C. Development of polynomial mode shape functions for continuous shafts with different end conditions[J/OL]. Journal of the Institute of Engineering, 2021, 16(1): 151-161. DOI: 10.3126/jie.v16i1.36653.

[8] Chhantyal B, Adhikari M, Chaudhary B B, et al. Use of polynomial mode shape function in free vibration analysis of cantilever Pelton turbine[J/OL]. Kathford Journal of Engineering and Management, 2024, 4(1): 92-101. DOI: 10.3126/kjem.v4i1.75499.

[9] Tazabekova A, Adair D, Ibrayev A, et al. Free vibration calculations of an Euler-Bernoulli beam on an elastic foundation using He's variational iteration method[C/OL]// Wu W, Yu H S. Springer Series in Geomechanics and Geoengineering: Proceedings of China-Europe Conference on Geotechnical Engineering. Cham: Springer International Publishing, 2018: 1022-1026. DOI: 10.1007/978-3-319-97115-5_30.

[10] Yoon D Y, Park J H. Adaptive polynomials for the vibration analysis of an L-Type beam structure with a free end[J/OL]. Journal of Marine Science and Engineering, 2021, 9(3): 300. DOI: 10.3390/jmse9030300.

[11] Ledda L, Greco A, Fiore I, et al. Closed-form exact solution for free vibration analysis of symmetric functionally graded beams[J/OL]. Symmetry, 2024, 16(9): 1206. DOI: 10.3390/sym16091206.

[12] Leung A Y T, Zhu B. Fourier p-elements for curved beam vibrations[J/OL]. Thin-Walled Structures, 2004, 42(1): 39-57. DOI: 10.1016/S0263-8231(03/00122-8.

[13] Rao S S. Mechanical vibrations[M]. Pearson Education, 2017.

[14] Meirovitch L. Elements of vibration analysis[M]. McGraw-Hill, 1986.

[15] Luintel M C. Textbook of mechanical vibrations[M]. Springer Nature Singapore, 2023.